RSC Advances

PAPER

View Article Online
View Journal | View Issue

Cite this: *RSC Adv.*, 2024, **14**, 15691

Innovation of 6-sulfonamide-2*H*-chromene derivatives as antidiabetic agents targeting α-amylase, α-glycosidase, and PPAR-γ inhibitors with *in silico* molecular docking simulation†

Hamdy Khamees Thabet, *[a] Ahmed Ragab, *[b] Mohd Imran,[c] Mohamed Hamdy Helal,[a] Saleh Ibrahim Alaqel,[c] Ahmed Alshehri,[de] Abida Ash Mohd,[c] Saleh Saad Alshammari,[a] Yousry A. Ammar [b] and Moustafa S. Abusaif [b]

A new series of 2-imino or 2-oxo-2*H*-chromene-6-sulfonamide derivatives **2–9** with potential antidiabetic activity were designed and synthesized. The new 6-sulfonamide chromenes were synthesized by reacting 3-formyl-4-hydroxybenzenesulfonyl chloride with activated methylene derivatives in the presence of ammonium acetate as a catalyst. The structure of the products was confirmed by spectroscopic analysis. All the designed derivatives **2–9** were evaluated for their activity against α-amylase and exhibited inhibitory percentage values higher than 93% at 100 μg mL^{-1}. Additionally, the IC_{50} values represented a variable degree of activity with two derivatives **2** and **9** exhibiting the most promising derivative results with IC_{50} values of 1.76 ± 0.01 and 1.08 ± 0.02 μM, respectively, compared to Acarbose (IC_{50} = 0.43 ± 0.01 μM). Additionally, these derivatives showed potency against the α-glucosidase enzyme with IC_{50} values of 0.548 ± 0.02 and 2.44 ± 0.09 μg mL^{-1}, compared to Acarbose (0.604 ± 0.02 μg mL^{-1}). Moreover, the *in vitro* PPAR-γ transactivation assay revealed that chromene-6-sulfonamide derivatives **2** and **9** exhibited potential PPAR-γ activity with IC_{50} values of 3.152 ± 0.03 and 3.706 ± 0.32 μg mL^{-1}, respectively, compared to Pioglitazone (4.884 ± 0.29 μg mL^{-1}). This indicates that these derivatives have insulin sensitivity and glucose metabolism activity. The *in silico* ADMET prediction showed that these derivatives have an acceptable range of oral bioavailability, drug-likeness, and a safe toxicity profile, including being non-cytotoxic, non-mutagenic, non-immunotoxic, and non-carcinogenic. Finally, computational docking analysis demonstrated the ability of these derivatives to interact with α-amylase, α-glucosidase, and PPAR-γ enzymes, with confirmed successful placement due to good binding energy values and various interactions within the pocket.

Received 21st March 2024
Accepted 9th May 2024

DOI: 10.1039/d4ra02143f

rsc.li/rsc-advances

1. Introduction

One of the most prevalent metabolic diseases is diabetic mellitus, which causes hyperglycemia due to defective insulin action or secretion, and this disease affects 451 million people worldwide (aged 18–99 years), according to the World Health Organization.[1,2] The number of patients with diabetes is expected to increase to 693 million by 2045, according to the International Diabetes Federation (IDF).[3] It has been reported that diabetes complications are associated with alterations in the body's antioxidant defense system, increased oxidative stress, and dyslipidemia.[3] Many studies have shown that diabetes complications affect 20 to 90.5% of the population.[4,5] Diabetes mellitus can be divided into four types: Type I diabetes mellitus, Type II diabetes mellitus, gestational diabetes mellitus (GDM), and finally, specific DM (cystic fibrosis diabetes, drug-induced diabetes, monogenic diabetes, and latent autoimmune diabetes in adults).[6] It has been shown that diabetes mellitus can cause ketoacidosis and hyperosmolarity[7] and chronic complications, such as peripheral and cerebrovascular disease, foot ulcers, retinopathy, and renal impairment.[8] It is still unknown how to cure diabetes mellitus, but there are ways to manage it, including taking oral anti-diabetic drugs and insulin and modifying your diet.[9] Moreover, in some cases,

[a]*Department of Chemistry, College of Sciences and Arts, Northern Border University, Rafha, 91911, Saudi Arabia. E-mail: Hamdy.salem@nbu.edu.sa*

[b]*Department of Chemistry, Faculty of Science (Boys), Al-Azhar University, Nasr City, 11884, Cairo, Egypt. E-mail: ahmed_ragab@azhar.edu.eg; Ahmed_ragab7@ymail.com*

[c]*Department of Pharmaceutical Chemistry, College of Pharmacy, Northern Border University, Rafha 91911, Saudi Arabia*

[d]*Department of Pharmacology and Toxicology, College of Pharmacy, Northern Border University, Rafha 91911, Saudi Arabia*

[e]*Department of Pharmacology, College of Clinical Pharmacy, Imam Abdulrahman Bin Faisal University, King Faisal Road, Dammam 31441, Saudi Arabia*

† Electronic supplementary information (ESI) available. See DOI: https://doi.org/10.1039/d4ra02143f

medicinal plants may provide an alternative method of treating diabetes mellitus.[10] The most common long-term health complications associated with diabetes include renal failure, neurologic complications, cerebrovascular disease, limb amputation, coronary artery disease, blindness, and premature death.[11,12] Most patients who take oral hypoglycemic medications suffer from gastrointestinal abnormalities, which affect more than half of patients when they are administered α-glucosidase and α-amylase inhibitors. Unabsorbed carbohydrates produce intestinal gas (colon gases), resulting in abdominal bloating, cramps, flatulence, and diarrhea.[13] These chemotherapeutic medications are not recommended for people with gastrointestinal problems, whether acute or chronic, hepatic dysfunction, and renal impairment.[14] Besides, to develop effective antidiabetic agents, we need to understand the adverse effects of these agents.[15]

Coumarin is a heterocyclic compound containing one oxygen atom in its bicyclic ring and exhibited extensive application in designing new potent therapeutic molecules.[16] Coumarine naturally occurs in several plants, including green tea, tonka beans, yellow sweet clover, chicory, lavender, and cassia.[17] Researchers and drug developers prefer coumarin compounds due to their advantages of multiple targets and low toxicity. Coumarin and its derivatives have antimutagenic, antiviral, antioxidant,[18] antibacterial,[19] and anticancer activities.[18,20] Moreover, the coumarin derivatives exhibited many bioactive potentials against monoamine oxidase, carbonic anhydrase, cholinesterase, urease, topoisomerase, lipoxygenase, alkaline phosphatase, histone deacetylase, α-glucosidase, and cyclooxygenase.[21] Additionally, many coumarin derivatives inhibit the α-glucosidase and α-amylase.[22,23] The extraction of Anacardiumouest Linn plant containing coumarins and terpenoids was shown to lower blood glucose levels in diabetic rats.[24] Besides, umbelliferone (7-hydroxycoumarin) is used to reduce blood glucose levels.[25,26] H. Sun *et al.*, synthesized new coumarin–flavonoid hybrids, as compound **I** that displayed glucosidase inhibitory activity with IC_{50} value of 1.47 ± 0.07 μM (Acarbose = 224.70 ± 14.14) and amylase with IC_{50} value of 6.89 ± 1.17 μM (Acarbose = 2.72 ± 0.30 μM).[27] Asgari *et al.*, developed a new bis-coumarin derivatives conjugated with 1,2,3-triazole nucleus to exhibit IC_{50} values of compound **II** (IC_{50} = 13.0 ± 1.5 μM) and compound **III** (IC_{50} = 16.4 ± 1.7 μM) against α-glucosidase inhibitory activity.[28] In addition, Elahabaadi *et al.*, modified coumarin with dithiocarbamate and found that the introduction of a nitro group at *meta* or *para* position at the phenyl ring of carbamate moiety led to high activity against α-glucosidase enzyme with IC_{50} values of for compound **IV** (IC_{50} = 101.6 ± 4.7 μM) and compound **V** (IC_{50} = 85.0 ± 4.0 μM).[29] Channabasappa *et al.*, synthesized new chorine with triazole fragment compound **VI**, demonstrating inhibitory activity to a-amylase with IC50 = 4.11 μM compared to Acarbose = 2.66 μM (ref. 23) Fig. 1.

Furthermore, the scientific community's interest became more attractive to the sulfonamide ($-SO_2NH_2$) core due to the wide variety of biological activity, such as anti-HIV, antimalarial, antithyroid, anticancer, high ceiling diuretic, insulin-releasing antidiabetic, carbonic anhydrase activity, and antimicrobial activity.[30–36] Recently, in 2022, the FDA approved some new sulphonamides as Mitapivat is a pyruvate kinase activator (used to treat hemolytic anemia),[37] Baricitinib as a selective Janus Kinase 1 (JAK 1) inhibitor (used to treat atopic dermatitis and severe rheumatoid arthritis),[38] Vonoprazan is an acid blocker for potassium-competitive (used to treat *H. pylori*), and Omidenepag isopropyl used to reduce the intraocular pressure for glaucoma patients.[28]

As a result of all the findings above, we urgently need additional drugs to compensate for the shortcomings of current drugs. Moreover, modification of the bioactive core to design

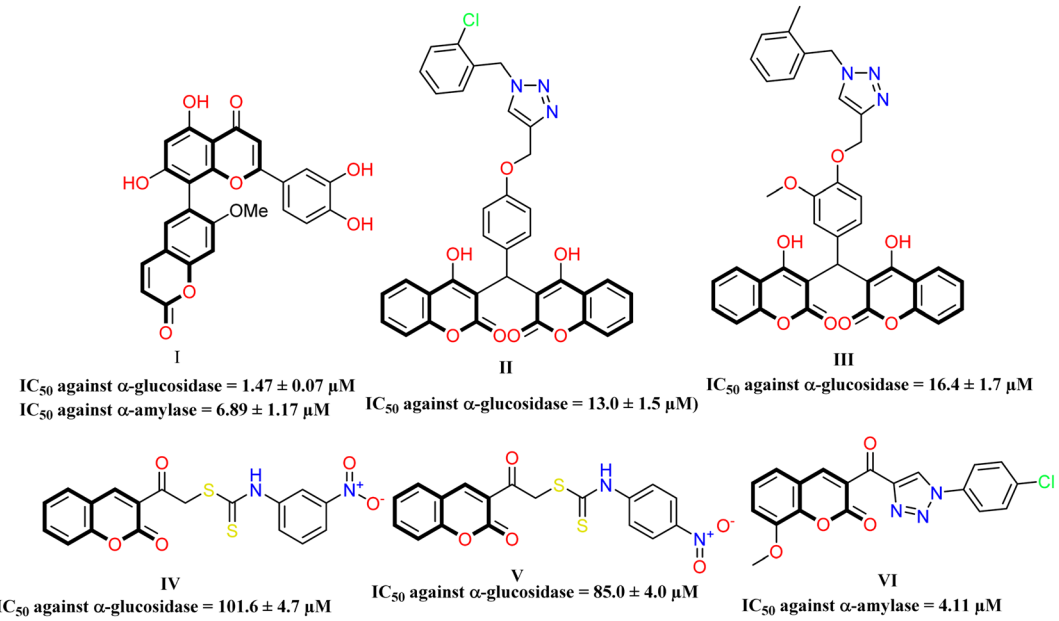

Fig. 1 Structure of the previously reported chromone derivatives as anti-diabetic agents as α-glucosidase and α-amylase inhibitors.

a new heterocyclic for a specific target is our research group goal.[39–41] Herein, this article synthesized a new 2*H*-chromene 6-sulfonamide. Moreover, all the designed derivatives are chosen to investigate the *in vitro* α-amylase inhibitory activity. The most active members were also used for further evaluation against α-glycosidase and PPAR-γ. Finally, the *in silico* ADMET and docking simulation was undertaken to determine the oral bioavailability, toxicity, and binding mechanism, including the interacting groups inside the active site of the pocket.

2. Results and discussion

2.1. Chemistry

Due to the high simplicity, low molecular weight, and significant reactivity of 3-formyl-4-hydroxybenzenesulfonyl chloride (**1**), the authors planned to use it as a starting material to construct and build up a novel bioactive chromene sulphonamide derivative. As a highly pure compound, the starting material (**1**) was obtained from ChemSpider with ID: 74821554. Also, the starting material included two electrophile active centers, known as the carboxaldehyde and the sulfonyl chloride groups. Meanwhile, the sulfonyl chloride group is more highly reactive toward some nucleophiles than the carboxaldehyde function, but this reactivity is not controlled in most cases. Moreover, the preparation of 3-formyl-4-hydroxybenzenesulfonamide is the main target for most chemists and biologists due to the high use of substituted benzene sulphonamide moiety (Ar–SO_2NH_2) that exhibited many biological activities, such as anti-bacterial agent,[42] anti-cancer agent,[43] anti-Alzheimer disease,[44] anti-diabetics,[45] and anti-inflammatory.[46] Unluckily, the synthetic pathways for preparing 3-formyl-4-hydroxybenzenesulfonamide as an intermediate are tricky and incompletely successful due to impurities and low yield percentage. This reason is explained through the reaction of 3-formyl-4-hydroxybenzenesulfonyl chloride (**1**) with ammonia (NH_3) which produced mixtures of the desired 3-formyl-4-hydroxybenzenesulfonamide (low yield) and undesired 4-hydroxy-3-(iminomethyl)benzene-sulfonamide (high yield). Therefore, the authors planned to produce the target bioactive materials *via* a one-pot three components reaction: 3-formyl-4-hydroxybenzenesulfonyl chloride (**1**), different activated methylene, and ammonium acetate (CH_3COONH_4). Additionally, the ammonium acetate used in this reaction act as a reagent to produce the sulphonamide moiety (–SO_2NH_2) and as a catalytic base to produce the cyclic chromene moiety in the presence of active methylene derivatives. The synthetic routes to prepare novel eight compounds are depicted in Schemes 1–3.

Firstly, the sulfonyl chloride derivative **1** is allowed to react with an equimolar amount of malononitrile in the presence of ammonium acetate *via* one-pot synthesis, yielding the corresponding 3-cyano-2-imino-2*H*-chromene-6-sulfonamide (**2**) as a high pure biomaterial (Scheme 1). The authors examined the physical properties of this product as a light-orange powder, in an excellent yield, with recorded melting point at 190–192 °C.

The chemical structure of the designed derivatives was confirmed using elemental analysis and spectral data. So, the IR data of compound **2** displayed the lack of absorption band at around 1680 cm^{-1} related to the carboxaldehyde group (–CHO). Also, the IR chart revealed new sharp stretching frequencies at ν 3414, 3335, 3233 cm^{-1} related to the NH_2 sulfonamide moiety and NH of the 2-imino chromene (C=NH), besides absorption bands at ν 2203, 1620, 1592, 1399, and 1185 cm^{-1} assignable to CN, C=NH, C=C, and SO_2 functions, respectively. Moreover, its ^{1}H NMR spectra showed two singlet signals in the down-field region at δ 8.76 and 9.39 ppm due to 4H-pyran and NH proton. Also, other singlet proton signals at δ 8.10 ppm due to the NH_2 function of sulfonamide moiety, aromatic protons as doublet signal at δ 7.32 ppm corresponding to the proton of H8-chromene with coupling constant (J = 8.8 Hz), doublet of doublet signal equivalent to H7-chromene at δ 7.86 ppm with coupling constant (J = 8.4, 4.0 Hz), and singlet signal at 8.39 ppm for the H5-chromene. Furthermore, the ^{13}C NMR spectrum represented only ten signals equivalent to the

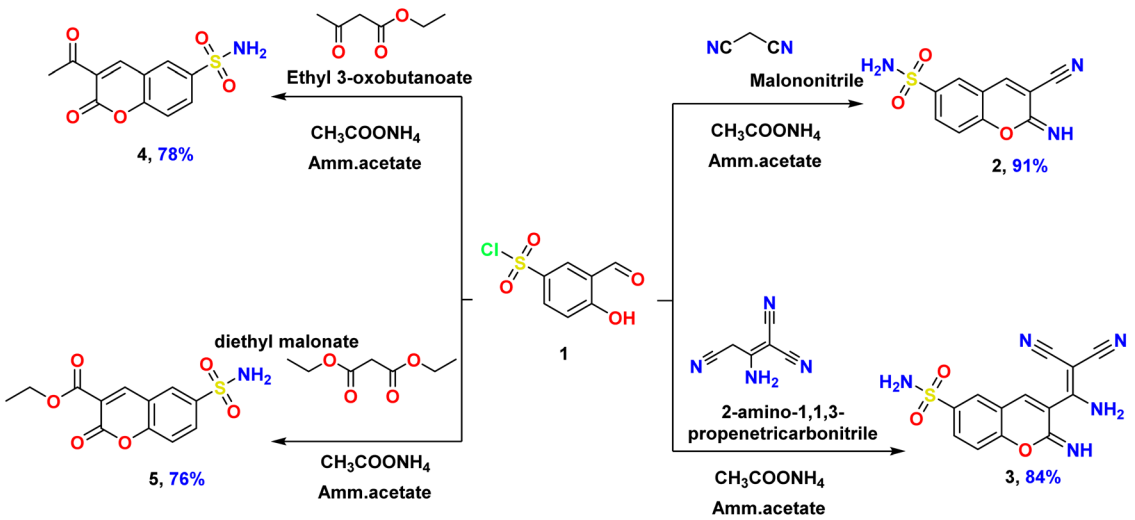

Scheme 1 Illustrate synthesis of 3-substituted-2-imino-2*H*-chromene-6-sulfonamide **2** & **3** and 3-substituted-2-oxo-2*H*-chromene-6-sulfonamide **4** & **5**.

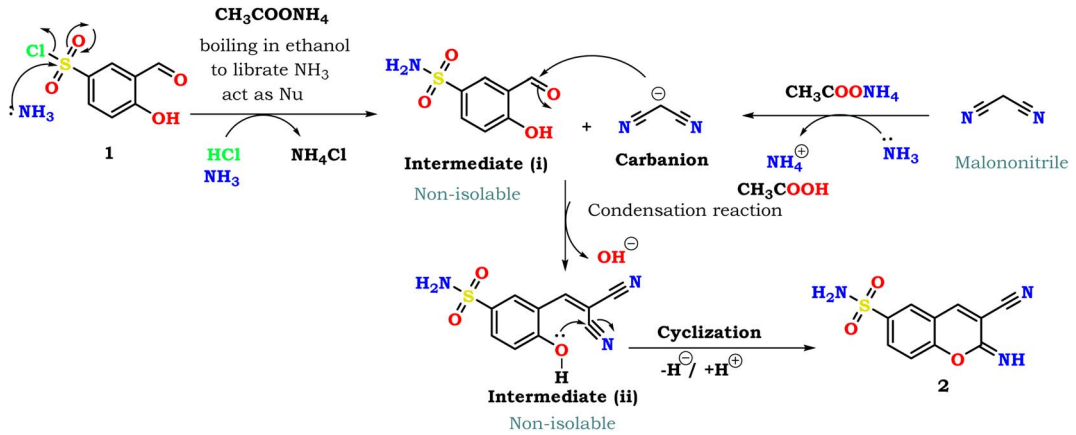

Scheme 2 Mechanism illustrated the synthetic approach of 3-cyano-2-imino-2*H*-chromene-6-sulfonamide **2**.

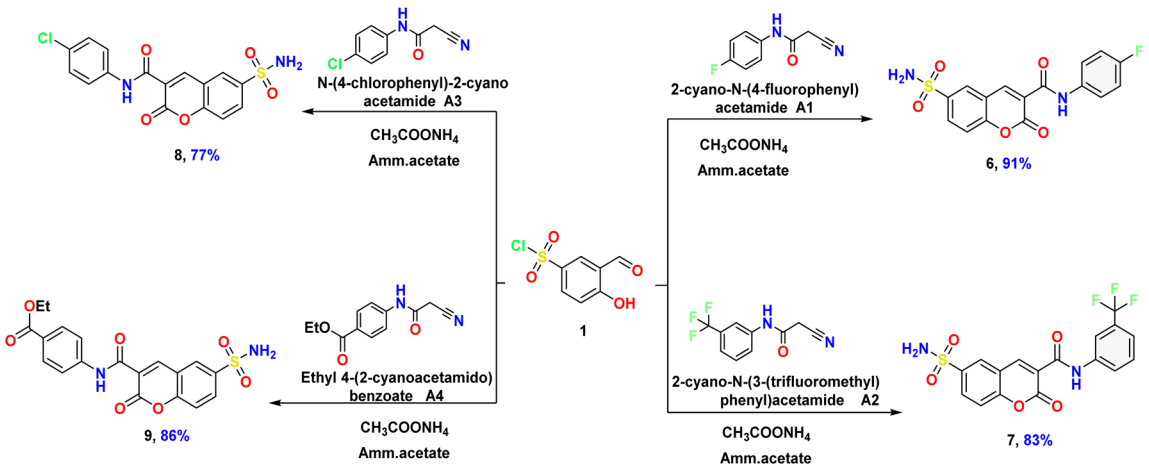

Scheme 3 Synthesis of the target *N*-(substitutedphenyl)-2-imino-6-sulfamoyl-2*H*-chromene-3-carboxamide **6–9**.

compound's total carbon atoms. The chart displayed signals at δ 96.01, 111.45, and 116.21 ppm related to carbon attached to the cyano group, C4 of pyran moiety, and cyano group, respectively. Although, in the downfield, other signals appeared at δ 138.12, 157.90, and 160.53 ppm related to carbon attached to sulfonamide moiety, carbon of (O–C=C), and carbon attached to imino function (C=NH), respectively. Besides signals of aromatic carbons in the middle region ranging between δ 118.25–131.91 ppm equivalent to four aromatic carbons.

In the same way, the other aliphatic activated methylene, such as 2-amino-1,1,3-propenetricarbonitrile, ethyl acetoacetate, and diethyl malonic acid is reacted with sulfonyl chloride salicylaldehyde **1** in the presence of ammonium acetate as a reagent and catalyst, afforded the corresponding 3-(1-amino-2,2-dicyanovinyl)-2-imino-2*H*-chromene-6-sulfonamide (**3**), 3-acetyl-2-oxo-2*H*-chromene-6-sulfonamide (**4**), and ethyl 2-oxo-6-sulfamoyl-2*H*-chromene-3-carboxylate (**5**), respectively (Scheme 1). The physical properties of the three bioactive materials were examined as pure materials and recorded in the experimental section. Also, the chemical structures of the same compounds were confirmed using elemental analysis and spectral data (IR, ^{1}H NMR, and ^{13}C NMR). For example, the IR analysis of 2-oxo-chromene derivative **5** confirmed the presence of strong absorption frequencies at ν 3183, 3064, 1765, and 1710 cm^{-1} related to the NH_2 of sulfonamide function, sp^2-CH group, and two carbonyl functions, respectively. Also, two frequencies of sulfonyl moiety (SO_2) at ν 1366, 1180 cm^{-1}. Continuously, ^{1}H NMR spectral of the same compound revealed new signals shielded in the up-field region as triplet signal at δ 1.29 ppm due to methyl protons of ester and quartet signals for methylene protons of ester at δ 4.27 ppm, as well as two significant singlet signals at δ 6.78 and 8.96 ppm related to the amino protons (NH_2) and 4*H*-pyran, respectively. Meanwhile, the aromatic protons appeared as two doublet signals at δ 7.61 and 7.92 ppm with the same coupling constant (J = 7.2 Hz) identified to H8 and H7-chromene, respectively. In addition, a singlet signal appears at δ 8.40 ppm H5-chromene. Furthermore, its ^{13}C NMR showed two signals at δ 13.99 and 60.58 ppm owing to carbons of the ester group, respectively. In addition, signals at δ 140.33, 156.58, 161.62, and 168.14 attributed to carbon attached to the sulfonyl group, carbon attached to (O–C=C), carbonyl of 2-oxo chromene, and carbonyl of the ester group, respectively.

As described in Scheme 2, the mechanistic pathway illustrated the synthetic pathway for producing the target bioactive

2-imino-2*H*-chromene derivative **2** as an example. Firstly, the mechanistic pathway moves forward *via* the nucleophilic addition of NH_3 (liberated from ammonium acetate) to the sulfonyl chloride group (SO_2Cl) to produce the sulfonamide moiety (intermediate i) by liberating the HCl that reacted with an excess of ammonia and formed ammonium chloride (NH_4Cl) as a by-product. Secondly, the ammonium acetate works as a source of ammonia that pulls a proton from malononitrile to form an active carbanion malononitrile, which is allowed to react with the formyl group in (intermediate i) *via* condensation reaction to yield the non-isolable (intermediate ii) that subsequently underwent intramolecular cyclization through nucleophilic attack of the phenolic hydroxyl (OH) group to the nitrile function to furnish the desired product 2.

Furthermore, the authors planned to produce some bioactive chromene containing carboxamide group *via* only a simple one-pot reaction process. According to the previous strategy, the starting material **1** is heated under reflux with different active cyano-acetanilide derivatives **A1–A4** in the presence of ammonium acetate and yielding the corresponding *N*-(substitutedphenyl)-2-imino-6-sulfamoyl-2*H*-chromene-3-carboxamide **6–8** (Scheme 3). The IR spectra of the carboxamide derivatives **6–8** revealed characteristic frequencies around ν 3431–3430 cm^{-1} related to the NH_2 and NH groups, besides two distinct bands related to the carbonyl groups of 2-oxo-chromene and the carbonyl of the amide function at ν 1727–1726, and 1655–1654 cm^{-1}, respectively. The ^1H NMR data of compound **6** exhibited four sharp singlet signals at δ 6.90, 8.43, and 10.46 ppm due to the amino protons, H4-chromene, and NH proton, respectively. The ^{19}F NMR spectra of compounds **6** and **7** revealed signals at δ −118.03 and −61.28 ppm related to C–F and CF_3, respectively, and these values fall within the range of the reported values.[47,48]

Finally, the bioactive material ethyl 4-(2-oxo-6-sulfamoyl-2*H*-chromene-3-carboxamido)benzoate (**9**) was isolated through the reaction of compound **1**, ethyl 4-(2-cyanoacetamido)benzoate (**A4**), and ammonium acetate in ethanolic solution under reflux condition for 5 hs and in the presence of ammonium acetate as a catalyst. In an acceptable yield, the compound is isolated as a pale-orange powder with melting point = 233–235 °C. The IR spectra viewed bands at ν 3430, 1726, and 1655 cm^{-1} due to NH_2, carbonyl of 2-oxo chromene, and the carbonyl of the amide function, respectively. Its ^1H NMR data displayed the two signals in the up-field region at δ 1.24 and 4.18 ppm corresponding to the ester protons as a triplet and quartet splitting and signals de-shielded at δ 5.91, 7.99, and 10.23 ppm assignable to the amino of sulfonamide, H4-chromene, and NH amide protons, respectively. Besides, the aromatic protons ranged from δ 6.92–7.60 ppm. The ^{13}C NMR spectra of the same compound displayed significant signals at δ 14.76, 61.03, 157.58, 163.46, and 166.20 ppm, equivalent to methyl carbon, methylene carbon, carbonyl of 2-oxo chromene, amide carbonyl carbon, and carbonyl of ester group respectively.

2.2. Antidiabetic activity

2.2.1. *In vitro* α-Amylase inhibitory activity with structure activity relationship. The synthesized 6-sulfonamide chromene derivatives **2–9** were screened as α-amylase inhibitors at 100 μg mL^{-1}. The results of the tested chromene derivatives exhibited a significant inhibitory percentage (IP) ranging between 93.4–96.6% compared to Acarbose IP = 96.5%, indicating that these derivatives can be used as hypoglycemic agents (Table 1). Moreover, the designed derivatives were evaluated for their inhibitory activity by determining the IC_{50} values by (μM) compared to Acarbose, and the results are summarized in Table 1. The obtained IC_{50} values exhibited variable degrees of inhibition at the micromolar level. Additionally, all the tested chromene derivatives revealed α-amylase inhibitory activity with IC_{50} values lower than 10 μM, except compounds **3** and **5**.

As represented in Table 1, the 2-oxo-6-sulfamoyl-2*H*-chromene-3-carboxamide derivative **9** emerged the most active hypoglycemic agent by inhibiting the α-amylase enzyme with IC_{50} value of 1.08 ± 0.02 μM. In addition, the 3-cyano-2-imino-2*H*-chromene-6-sulfonamide (**2**) revealed the second active member among the synthesized derivatives with IC_{50} value of 1.76 ± 0.01 μM compared to Acarbose (IC_{50} = 0.43 ± 0.01 μM). The activity of the synthesized derivatives was displayed due to two positions only in the chromene nucleus: the imino or carbonyl at position two and the fragments at position three (cyano, vinyl, ethyl acetate, acetyl, and carboxamide). Firstly, for the imino group, grafting the cyano as compound **2** increases the inhibitory potency by nearly 8.31-fold when replaced with 1-amino-2,2-dicyanovinayl derivative **3**, indicating that an increase in the conjugation system at position three decreases the activity.

On the other hand, the IC_{50} values displayed introducing the carboxamide moiety with different substituents at position three of chromenes **6–9** demonstrated inhibitory activity with IC_{50} values ranging from 1.08 ± 0.02 to 4.39 ± 0.06 μM (*i.e.*, below 5 μM). Generally, introducing the electron-withdrawing groups at the *para* position is more effective than the *meta* position. Additionally, introducing *N*-(4-fluorophenyl)-3-carboxamide fragment showed IC_{50} value of 2.11 ± 0.03 μM, while replacing the fluoro with chloro atom decreased the α-amylase activity enzyme with IC_{50} value of 4.23 ± 0.06 μM. Further, the replacement of *N*-(4-fluorophenyl)-3-carboxamide in compound **6** with -*N*-(3-(trifluoromethyl)phenyl), as showed in compound **7** to

Table 1 *In vitro* α-amylase activity of the newly synthetized 6-sulfonamide chromene derivatives **2–9**

	The α-amylase activity	
Cpd no.	Inhibitory percentage at 100 μg mL^{-1}	IC_{50} ± SD (μM) DF = 100
2	96.1	1.76 ± 0.01
3	96	14.62 ± 0.16
4	94.2	8.55 ± 0.31
5	93.4	32.58 ± 0.33
6	95.4	2.11 ± 0.03
7	96.2	4.39 ± 0.06
8	95.4	4.23 ± 0.06
9	96.6	1.08 ± 0.02
Acarbose	96.5	0.43 ± 0.01

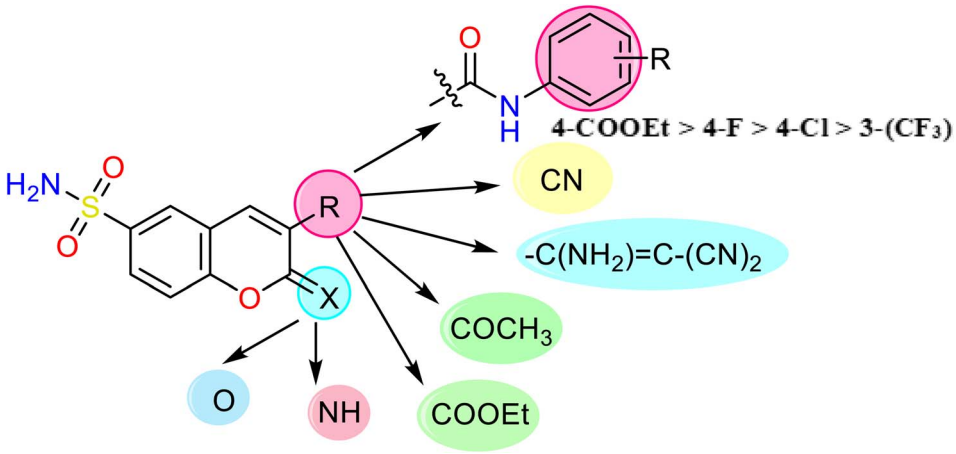

Fig. 2 General structure with different substituents that exhibited the activity and SAR study of the newly designed chromene derivatives **2–9**.

increase the number of fluorine atoms, reduces the activity with nearly two folds and demonstrated IC_{50} value of 4.39 ± 0.06 μM. To our surprise, replacing the halogenated atoms (4-F and 4-Cl) or 3-trifluoromethyl with ethyl carboxylate group (COOEt) causes an increase in the activity with IC_{50} value of 1.08 ± 0.02 μM. Furthermore, replacing the carboxamide on 2-oxo-2*H*-chromene pharmacophore with ethyl carboxylate or acetyl group causes reduction in the activity with IC_{50} values for compound **4** (IC_{50} = 8.55 ± 0.31 μM) and compound **5** (IC_{50} = 32.58 ± 0.33 μM) indicating the presence of amide group and its aromatic moiety is important in activity Fig. 2.

Finally, the designed chromene demonstrated α-amylase inhibitory activity. Additionally, the SAR study showed that the carboxamide in position three and the carbonyl group in position two are essential in reducing glucose levels by inhibiting the α-amylase enzyme. Moreover, any change in these two groups by introducing esters or acetyl instead of carboxamide doesn't enhance the α-amylase activity, except for inserting a cyano group at position three and replacing carbonyl with an imino group.

2.2.2. *In vitro* α-glucosidase activity. The diabetic activity of the most active 6-sulfonamide-2*H*-chromene derivatives **2** and **9** is further estimated by α-glucosidase assay. Firstly, the inhibitory percentage at 10 μg mL^{-1} showed that the 2*H*-chromene derivatives **2** and **9** expressed IP values of 90.7 and 83.8% in comparison to Acarbose IP = 90.1%. Additionally, using five concentrations from the inhibitors (10, 5, 1, 0.1, and 0.01 μg mL^{-1}), the IC_{50} values were calculated Table 2. The 3-cyano-2-imino-2*H*-chromene-6-sulfonamide (**2**) showed inhibitory potential to α-glucosidase with IC_{50} value of 0.548 ± 0.02 μg mL^{-1} higher than Acarbose as a positive FDA-approved drug (IC_{50} = 0.604 ± 0.02 μg mL^{-1}). In addition, the ethyl 4-(2-oxo-6-sulfamoyl-2*H*-chromene-3-carboxamido)benzoate (**9**) exhibited lower α-glucosidase activity with IC_{50} value of 2.44 ± 0.09 μg mL^{-1}.

2.2.3. *In vitro* peroxisome proliferator-activated receptor gamma (PPAR-γ). To assess the impact of the most active 6-sulfonamide-2*H*-chromene derivatives **2** and **9** on insulin sensitivity and glucose metabolism, the *in vitro* PPAR-γ transactivation assay was evaluated. Pioglitazone was used as a positive control. The results reported that the 3-cyano-2-imino-2*H*-chromene-6-sulfonamide (**2**) and 2-oxo-6-sulfamoyl-2*H*-chromene-3-carboxamide derivative **9** showed notable potency with IC_{50} value of 3.152 ± 0.03 and 3.706 ± 0.32 μg mL^{-1} with nearly 1.55 and 1.32 folds compared to Pioglitazone (IC_{50} = 4.884 ± 0.29 μg mL^{-1}), respectively Table 3.

2.3. *In silico* toxicity and drug likeness prediction

Recently, there has been great concern about the toxicity of developed molecules to be used as candidate drugs,[49,50] so in this section, we study the toxicity prediction of the most active derivatives **2** and **9**, as well as positive controls (Acarbose and Pioglitazone). The toxicity prediction was performed by constructing the structure using the previously reported method,[51,52] where the structure was exported to the ProTox-II prediction web server tool (**https://tox-new.charite.de/protox_II**/last access 28/4/2024).

Table 2 *In vitro* α-glucosidase activity of the most active 6-sulfonamide chromene derivatives **2** and **9**

	α-Glucosidase activity	
Cpd no.	Inhibitory potential at 10 μg mL^{-1}	IC_{50} ± SD (μg mL^{-1}) DF = 100
2	90.7	0.548 ± 0.02
9	83.8	2.44 ± 0.09
Acarbose	90.1	0.604 ± 0.02

Table 3 *In vitro* PPAR-γ activity of the most active 6-sulfonamide chromene derivatives **2** and **9**

	PPAR-γ	
Cpd No	IC_{50} ± SD (μg mL^{-1})	Folds
2	3.152 ± 0.03	1.55
9	3.706 ± 0.32	1.32
Pioglitazone	4.884 ± 0.29	1

The most active 6-sulfamoyl-2*H*-chromene derivatives (**2** and **9**) and positive controls (Acarbose and Pioglitazone) exhibited a safe profile to non-cytotoxic, non-mutagenic, non-immunotoxic (except for Acarbose that showed activity with a probability value of 0.99), and non-carcinogenic. Fortunately, 3-cyano-2-imino-2*H*-chromene-6-sulfonamide (**2**) revealed non-hepatotoxic activity compared to other tested compound **9** and positive controls. Moreover, 6-sulfamoyl-2*H*-chromene derivatives **9** and Pioglitazone belong to class IV in the toxicity class with LD_{50} expected values of 1000 mg kg^{-1}, while the 2-imino-2*H*-chromene-6-sulfonamide derivative **2** (class V with LD_{50} = 4870 mg kg^{-1}) and Acarbose (class VI with LD_{50} = 24 000 mg kg^{-1}). The tested derivatives were predicted to be inactive members to in term of heat shock factor response element (HSE) (increase in temperature), mitochondrial membrane potential (MMP), and phosphoprotein p53 gene (Table 4).

Moreover, our work was extended to study the prediction of additional toxicity items based on ProTox-3.0 – prediction of toxicity of chemicals web tools. The results showed that the most active 6-sulfamoyl-2*H*-chromene derivatives **2** and **9** exhibited inactive properties for neurotoxicity, cardiotoxicity, ecotoxicity, clinical toxicity, and nutritional toxicity, except for ethyl 4-(2-oxo-6-sulfamoyl-2*H*-chromene-3-carboxamido)benzoate (**9**) which showed activity for neurotoxicity and clinical toxicity with probability values of 0.59 and 0.55, respectively. Additionally, Acarbose and Pioglitazone demonstrated safe profiles for ecotoxicity and nutritional toxicity with high probability values. In contrast, Pioglitazone showed active properties for neurotoxicity ($P \sim 0.83$) and clinical toxicity ($P \sim 0.86$). On the other hand, Acarbose

Table 4 *In silico* toxicity prediction of most active 6-sulfamoyl-2*H*-chromene derivatives (**2** and **9**) and positive controls (Acarbose and Pioglitazone)[a]

		Most active 6-sulfamoyl-2*H*-chromene derivatives (**2** and **9**) and positive controls Acarbose and Pioglitazone			
Oral toxicity prediction		2	9	Acarbose	Pioglitazone
		Oral toxicity prediction			
ProTox-II prediction	LD_{50} mg kg^{-1}	4870	1000	24 000	1000
	Toxicity class	V	IV	VI	IV
	Hepatotoxicity	Inactive	Active	Active	Active
		0.66	0.53	0.65	0.51
	Carcinogenicity	Inactive	Inactive	Inactive	Inactive
		0.50	0.62	0.84	0.52
	Immunotoxicity	Inactive	Inactive	Active	Inactive
		0.99	0.99	0.99	0.89
	Mutagenicity	Inactive	Inactive	Inactive	Inactive
		0.72	0.65	0.76	0.71
	Cytotoxicity	Inactive	Inactive	Inactive	Inactive
		0.80	0.74	0.70	0.73
	Neurotoxicity	Inactive	Inactive	Inactive	Active
		0.75	0.84	0.60	0.83
	Nephrotoxicity	Inactive	Active	Active	Inactive
		0.52	0.59	0.80	0.50
	Cardiotoxicity	Inactive	Inactive	Active	Inactive
		0.74	0.54	0.60	0.52
	Ecotoxicity	Inactive	Inactive	Inactive	Inactive
		0.76	0.81	0.66	0.58
	Clinical toxicity	Inactive	Active	Active	Active
		0.57	0.55	0.65	0.86
	Nutritional toxicity	Inactive	Inactive	Inactive	Inactive
		0.70	0.60	0.52	0.56
	Heat shock factor response element (HSE)	Inactive	Inactive	Inactive	Inactive
		0.97	0.97	0.98	0.98
	Mitochondrial membrane potential (MMP)	Inactive	Inactive	Inactive	Inactive
		0.78	0.78	0.97	0.57
	Phosphoprotein (tumor suppressor) p53	Inactive	Inactive	Inactive	Inactive
		0.90	0.93	0.97	0.91
ADMETLab2.0	Eye corrosion	−3	−3	−3	−3
	Eye irritation	−2	−3	−3	−3
	Respiratory toxicity	+2	−3	−3	−2
	Skin sensitization	−3	−3	−3	−1
	Half life time ($t_{1/2}$ = h)	0.669	0.154	0.835	0.311
	Clearance (mL min^{-1} kg^{-1})	1.737	0.639	0.681	8.271

[a] For ADMETlab2.0 the values described as: −3 = (high safe with probability ~ 0.0–0.1); −2 = (moderate safe with probability ~ 0.1–0.3); −1 = (safe with probability ~ 0.3–0.7); +1 = (low risk with probability ~ 0.5–0.7); +2 = (moderate risk with probability ~ 0.7–0.9); and +3 = (high risk with probability ~ 0.9–1.0).

exhibited active properties for nephrotoxicity ($P \sim 0.80$), cardiotoxicity ($P \sim 0.60$), and clinical toxicity ($P \sim 0.65$).

Furthermore, some other important toxicity prediction items and excretion properties such as [half lifetime ($t_{1/2} = h$) and clearance (mL min^{-1} kg^{-1})] were predicted using ADMETLab2.0 web server (**https://admetmesh.scbdd.com/service/evaluation/index** last accessed 26/1/2024). The tested derivatives and drugs showed non-corrosive and non-irritant for the eye, non-sensitizer for the skin, and non-respiratory toxic with probability properties ranging from moderate to high safe, except for 3-cyano-2-imino-2*H*-chromene-6-sulfonamide (**2**) that demonstrated respiratory toxicity with probability value between 0.7-0.9 indicating moderate risk. The Pioglitazone exhibited the lowest safety profile with non-sensitizer to the skin (probability values $\sim$ 0.3–0.7) and an alarming pharmacophore related to the thiazole ring. Additionally, all tested compounds featured short half-time values from 0.154 to 0.835 h, as well as low clearance values ranging between 0.639 and 1.737 mL min^{-1} kg^{-1}, except for Pioglitazone which displayed a moderate clearance value of $\sim$8.271 mL min^{-1} kg^{-1} (Table 4).

The designed 6-sulfamoyl-2*H*-chromene derivatives and Pioglitazone do not violate the Lipinski rule (RO5), indicating that these derivatives in clinical trials tend to be shorter and, therefore, have a better chance of success. However, Acarbose doesn't obey RO5 due to three violations violations: MW > 500, NorO > 10, NHorOH > 5. Also, 2*H*-chromene derivatives **2** and Pioglitazone passed with the Veber rule, while 2*H*-chromene derivatives **9** and Acarbose failed due to TPSA > 140 Å. Additionally, the 6-sulfamoyl-2*H*-chromene derivatives **2** and **9** exhibited soluble properties with log *S* (ESOL) values of −2.06 and 3.46, respectively. On the other hand, they showed highly soluble properties log *S* (ESOL) = −2.13, while Pioglitazone showed moderate solubility log *S* (ESOL) = −4.31. For synthetic accessibility, the 2*H*-chromene derivatives (**2** and **9**) and Pioglitazone exhibited easy synthesis with values of 2.89, 3.21, and 3.46, respectively. Acarbose represented difficult synthetic accessibility with a probability of 7.34. All derivatives demonstrated good bioavailability scores with probability values ranging from 0.17 to 0.55 (Table 5).

2.4. *In silico* molecular docking simulation

To determine the conformation and ligand–protein interaction of the most active derivatives **2** and **9** that exhibited the activity with lower IC_{50} values on α-amylase, α-glucosidase, and PPAR-γ, the docking simulation carried out compared to the positive controls used in each *in vitro* study (Acarbose and Pioglitazone), as well as antidiabetic drugs have sulphonamide moiety *e.g.*, Chlorpropamide, Glibenclamide. The docking simulation was performed using Molecular Operating Environmental (MOE) 10.2009 software[53,54] inside the active site of α-amylase (PDB: 2QV4), α-glucosidase (PDB: 3w37), and PPAR-γ (PDB: 3SZ1).[55–57]

2.4.1. Ligand–protein complex interaction inside α-amylase (PDB: 2QV4). The docking simulation of most active 6-sulfamoyl-2*H*-chromene derivatives **2** and **9** inside the active site of α-amylase (PDB: 2QV4) exhibited binding energy $S = -8.88$ and -9.29 kcal mol^{-1} compared to the Acarbose as positive control and co-crystallized ligand ($S = -17.19$ kcal mol^{-1} with RMSD = 1.43 Å). The validation process showed five hydrogen bond donors (Thr201, Thr163, 2*Asp300, Tyr62, and Asn105), one hydrogen bond acceptor (His201), and many hydrophobic interactions between Acarbose and near amino acids inside the pocket, as well as ligand exposure that appears as blue color with background on the ligand structure (Fig. 3a, superimposable structure of co-crystallized ligand).

Table 5 Prediction of molecular properties, drug likeness and medicinal chemistry of 6-sulfamoyl-2*H*-chromene derivatives (**2** and **9**) and positive controls Acarbose and Pioglitazone[a]

		Most active 6-sulfamoyl-2*H*-chromene derivatives (**2** and **9**) and positive controls Acarbose and Pioglitazone			
		2	9	Acarbose	Pioglitazone
Test items		Molecular properties			
SwissADME	MLogP	−0.57	1.13	−6.94	2.01
	TPSA (Å^2)	129.32	154.15	321.17	93.59
	MW	249.25	416.40	645.60	356.44
	*n*HBA (NO)	6	8	19	4
	*n*HBD (OHNH)	2	2	14	1
	NRB	1	7	9	7
	Fraction Csp^3	0.00	0.11	0.92	0.32
	Drug likeness and medicinal chemistry prediction				
	Log *S* (ESOL)	−2.06	3.46	−2.13	−4.31
	Solubility	Soluble	Soluble	H. Soluble	M. Soluble
	PAINS	0	0	0	0
	Lead-likeness	No (1)	No (1)	No (2)	No (2)
	Synthetic accessibility	2.89	3.21	7.34	3.46
	Bioavailability score	0.55	0.55	0.17	0.55
	Lipinski rule (violation)	Yes (0)	Yes (0)	No (3)	Yes (0)
	Veber rule (violation)	Yes (0)	No (1)	No (1)	Yes (0)

[a] M. Soluble = moderately soluble; H. Soluble = highly soluble.

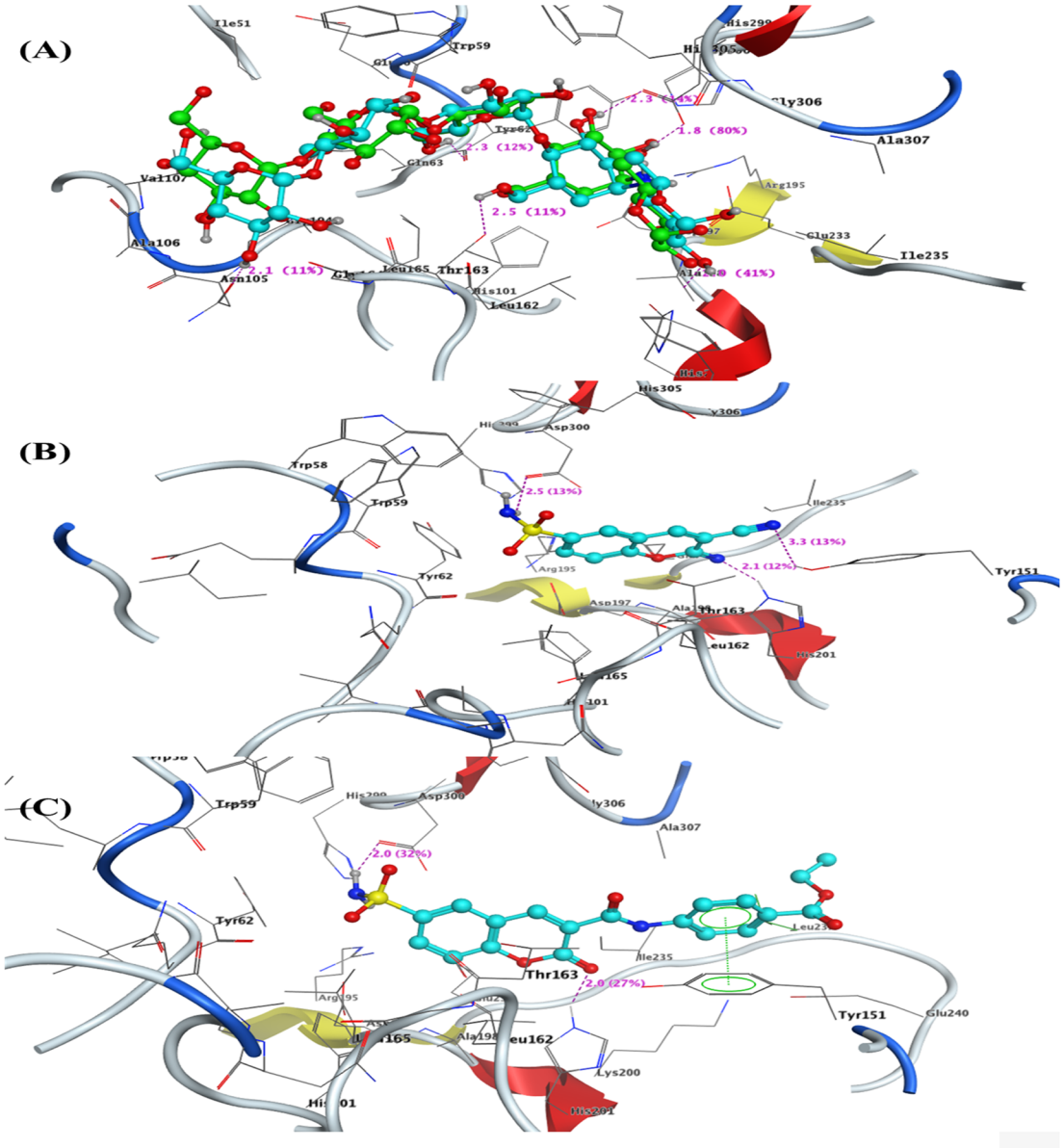

Fig. 3 3D interaction of (A) co-crystallized Acarbose as superimposable (green is the original pose, while turquoise is our pose), (B) compound **2**, and (C) compound **9** inside the active site of α-amylase (PDB: 2QV4).

The 3-cyano-2-imino-2*H*-chromene-6-sulfonamide (**2**) showed binding energy $S = -8.88$ kcal mol^{-1} and interacted with pocket through two sidechain H-bonds acceptor with Tyr151 with nitrogen of cyano group (3.3 Å and strength of 13%) and His201 with nitrogen of imino group at position two of chromene (2.1 Å and strength of 12%). Moreover, the amino acid residue Asp300 located on the sidechain formed H-bond donor with the amino group of sulfonamide moiety with a distance of 2.5 Å and strength of 13% (Fig. 3b). Additionally, this compound exhibited hydrophobic interactions with Glu233, Tyr58, and Tyr62. Meanwhile, the 2-oxo-6-sulfamoyl-2*H*-chromene-3-carboxamide **9** displayed the highest binding energy $S = -9.29$ kcal mol^{-1}, confirming the *in vitro* α-amylase's $IC_{50} = 1.08 \pm 0.02$ μM. Compound **9** demonstrated two H-bonds interaction with His201 (sidechain acceptor) and Asp300 (sidechain donor) as the interaction of co-crystallized ligands with bond lengths of 2.0 Å and strength of (27 and 32%), respectively. In addition, the compound's center is located over the phenyl ring of Tyr151, exhibiting arene–arene interaction and hydrophobic interaction inside the pocket (Fig. 3c). Moreover, the docking simulation of Chlorpropamide and Glibenclamide, as antidiabetic drugs with a sulphonamide moiety, exhibited higher binding energy than the designed derivatives **2** and **9**. Chlorpropamide showed a binding energy of $S = -2.99$ kcal mol^{-1}, with one hydrogen bond sidechain donor between the residue Asp300 and NH of the sulfonamide group ($NH–SO_2^-$), with a bond length of 2.0 Å and a strength of 14% Fig. S1 and S2.† On the other hand, Glibenclamide

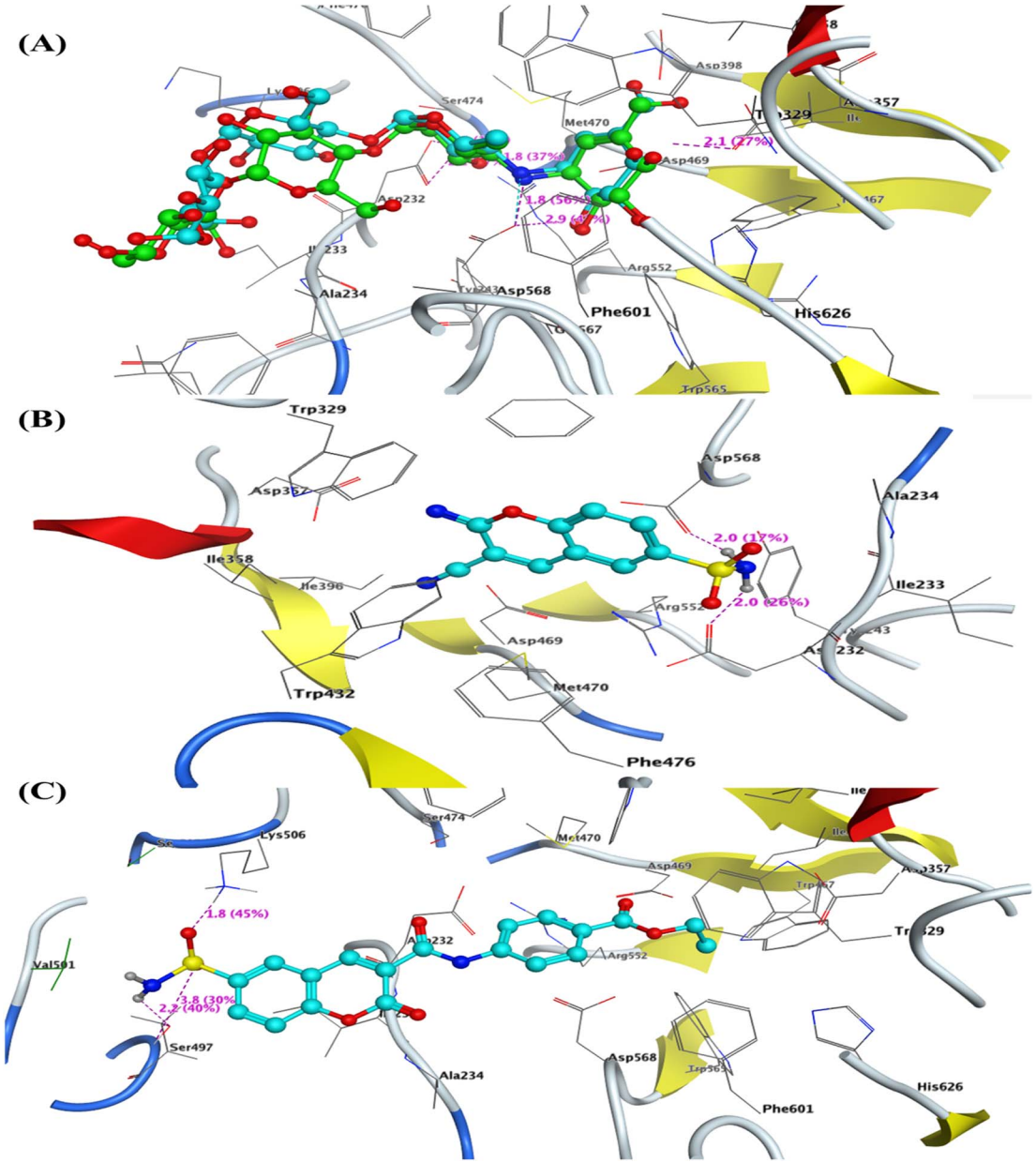

Fig. 4 3D interaction of (A) co-crystallized Acarbose as superimposable (green is the original pose, while turquoise is our pose), (B) compound **2**, and (C) compound **9** inside the active site of α-glucosidase (PDB: 3w37).

demonstrated a binding energy of $S = -4.98$ kcal mol^{-1} through an arene–arene interaction between the *m*-chloro phenyl group and Tro59 Fig. S3 and S4 (see ESI for figures).†

2.4.2. Ligand–protein complex interaction inside α-glucosidase (PDB: 3w37). The redocking process of Acarbose in the active site showed that the co-crystallized ligand possesses H-bond interactions with Asp357, 2*Asp232, 2*Asp568, and Arg552, besides many hydrophobic interactions, as described in Fig. 4a. The docking pose of 3-cyano-2-imino-2*H*-chromene-6-sulfonamide (**2**) inside α-glucosidase (PDB: 3w37) showed binding energy $S = -10.68$ kcal mol^{-1} through two H-bond donors with Asp568 and Asp232 with the amino group of sulfonamide group with a bond length of 2.0 Å and strength of 17 and 26%, respectively. Additionally, the hydrophobic interactions observed with residues (Tyr232, Ile233, phe601, Trp329, Trp329, and Trp432) and the ligand exposure displayed as blue shadow in 2D structure over the phenyl of chromene and sulfonyl group Fig. 4b. On the other hand, 2-oxo-6-sulfamoyl-2*H*-chromene-3-carboxamide derivative **9** demonstrated binding energy $S = -8.73$ kcal mol^{-1} with two H-bonds side-chain acceptors with the oxygen of sulfonyl group with Lys506 and Ser497 with a bond distance of 3.8 and 1.8 Å and strength of 30 and 45%, respectively. Further, compound **9** viewed some ligand exposure and hydrophobic interaction because it positioned slightly closer to many residues as (Ala232, Lys506, Asp232, Asp469, Trp432, Met470, Phe601, and Asp568) Fig. 4c. Additionally, the Chlorpropamide exhibited binding energy $S = -6.11$ kcal mol^{-1} with two hydrogen bonds sidechain acceptors.

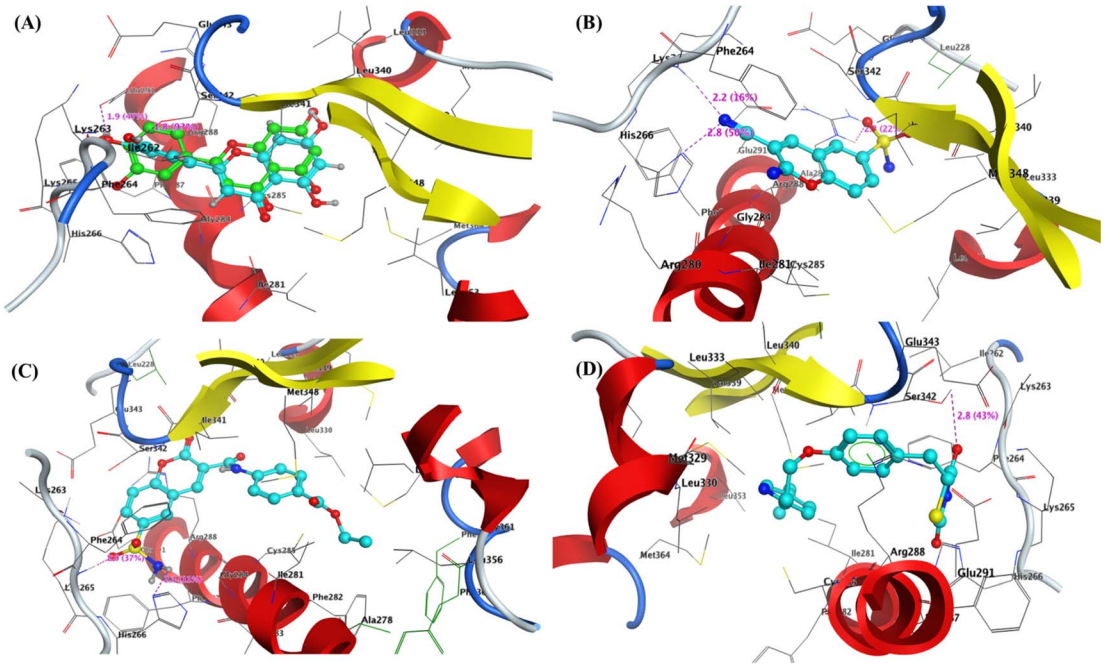

Fig. 5 3D interaction of (A) co-crystallized Ligand as superimposable (green is the original pose, while turquoise is our pose), (B) compound **2**, and (C) compound **9**, and (D) Pioglitazone inside the active site of PPAR-γ (PDB: 3SZ1).

The oxygen of SO_2 was bound to His626 with a bond length of 2.1 Å and a strength of 43%, while the oxygen of the carbonyl (amide group) formed a H-bond with the residue Arg552 with a distance of 2.3 Å and a strength of 46%, as well as many hydrophobic interactions inside the active site of the pocket Fig. S5 and S6.† The Glibenclamide interacted with the active site of the amino acid residues Lys506 and Arg552, forming hydrogen bond acceptors from the sidechain with the oxygen of SO_2 and the oxygen of the carbonyl with a distance of 2.2 Å (22%) and 2.4 Å (22%), respectively. Additionally, the urea derivative [$(-NH)_2$–C=O] and the sulfonamide group [–NH–SO_2^-] in the Glibenclamide exhibited ligand exposure with the pocket. They appeared blue color through the 2D diagram Fig. S7 and S8 (see ESI for figures).†

2.4.3. Ligand–protein complex interaction inside PPAR-γ (PDB: 3SZ1). In PPAR-γ (PDB: 3SZ1), the co-crystallized ligand (luteolin) displayed two hydrogen bond acceptors between the Ser342 and Glu291 with the two hydroxyl groups at phenyl ring attached at C2 of luteolin (2-(3,4-dihydroxyphenyl)-5,7-dihydroxy-4*H*-chromen-4-one) with bond length of 1.8 and 1.9 Å with strength of 93 and 47%, respectively Fig. 5a.

Furthermore, the most active 6-sulfamoyl-2*H*-chromene derivatives **2** and **9** showed the lowest binding energy (S = −13.64 and −12.67 kcal mol^{-1}) than Pioglitazone as positive control (−12.43 kcal mol^{-1}). The 3-cyano-2-imino-2*H*-chromene-6-sulfonamide (**2**) interacted with PPAR-γ with three hydrogen bond acceptors with residues Lys262 and His266 that interacted with the nitrogen of cyano group with a distance of 2.2 and 2.8 Å, while the third one displayed between the oxygen of sulfonyl group with Arg288 with a bond length of 2.2 Å and strength of 22%. The structure of compound **2** is located inside the pocket and formed hydrophobic interactions with (Leu228, Leu333, Leu340, Glu343, Ser342, Ile341, Phe264, and Gly284) Fig. 5b. Similarly, the 2-oxo-6-sulfamoyl-2*H*-chromene-3-carboxamide **9** exhibited two hydrogen bonds with residues Lys265 and His266 that bounded to oxygen and amino of sulfonamide (–SO_2NH_2) with bond lengths of 2.0 and 2.3 Å, respectively Fig. 5c. Finally, the Pioglitazone bounded to the common amino acid residue Ser342 with H-bond sidechain acceptor with the oxygen of carbonyl at C4 of thiadiazol-2,4-dione with bond length of 2.8 Å and strength of 43%. Besides, the Arg288 could interact with phenyl ring of Pioglitazone through arene–cation interaction Fig. 5d. For Chlorpropamide and Glibenclamide, it was found that the binding energy of these antidiabetic sulfonamide drugs exhibited binding energy S = −4.44 and −7.81 kcal mol^{-1}, respectively. Chlorpropamide displayed one hydrogen bond backbone acceptor between the residue Ser289 and oxygen of SO_2 with a bond length of 2.2 Å and strength of 38% Fig. S9 and S10.† On the other hand, Glibenclamide showed one hydrogen bond sidechain donor between the residue Ser289 and NH of sulfonamide with a bond length of 2.7 Å and strength of 32% Fig. S11 and S12 (see ESI figures).†

Finally, it can be concluded that the most active 6-sulfamoyl-2*H*-chromene derivatives **2** and **9** showed lower binding energy than Chlorpropamide and Glibenclamide as antidiabetic drugs have sulphonamide moiety against α-amylase, α-glucosidase, and PPAR-γ enzymes.

3. Conclusion

Herein, this article synthesized new 2*H*-chromene 6-sulfonamide by reaction of 5-sulfonyl salicylaldehyde with different reagents containing active methylene group in the presence of ammonium

acetate as a basic catalyst, where the reaction proceeded by condensation followed by intramolecular cyclization to afford the target compounds. Moreover, the *in vitro* α-amylase inhibitory activity was evaluated for all the designed derivatives. The 2-oxo-6-sulfamoyl-2*H*-chromene-3-carboxamide derivative **9** emerged as the most active hypoglycemic agent by inhibiting the α-amylase enzyme with IC_{50} value of 1.08 ± 0.02 μM, while the 3-cyano-2-imino-2*H*-chromene-6-sulfonamide (**2**) revealed the second active member among the synthesized derivatives with IC_{50} value of 1.76 ± 0.01 μM compared to Acarbose (IC_{50} = 0.43 ± 0.01 μM). Among the tested compounds, two derivatives exhibited good inhibitory activity and were used for further evaluation against α-glycosidase and PPAR-γ. Surprisingly, compounds **2** and **9** showed inhibitory potential to α-glucosidase with IC_{50} values of 0.548 ± 0.02 and 2.44 ± 0.09 μg mL^{-1} compared to Acarbose as a positive FDA-approved drug (IC_{50} = 0.604 ± 0.02 μg mL^{-1}). Further, the most active 6-sulfonamide-2*H*-chromenes **2** and **9** were potent agonists against PPAR-γ receptors with IC_{50} values of 3.152 ± 0.03 and 3.706 ± 0.32 μg mL^{-1} compared to Pioglitazone (IC_{50} = 4.884 ± 0.29 μg mL^{-1}). The *in silico* ADMET, including molecular properties, medicinal chemistry, drug-likeness properties, and toxicity prediction, were also studied. Finally, the docking simulation was performed on the active site of α-amylase, α-glycosidase, and PPAR-γ and determined the best conformation and, therefore, determined the binding energy and interaction types inside the pockets. The promising outcomes of most active derivatives encourage us to investigate further several enzymatic tests, including lipase, aldose reductase, DPP4, and assess more *in vivo* studies to improve efficacy, reduce potential side effects, *etc.*

4. Experimental

4.1. Chemistry

4.1.1. Materials. Reagents and starting ingredients were obtained from commercial sources and did not undergo additional purification before being utilized unless specified differently. The starting material 3-formyl-4-hydroxybenzenesulfonyl chloride (**1**) was obtained from ChemSpider with ID: 74821554. The other reagents sources are such as ammonium acetate CH_3COONH_4 (Fischer Scientific USA), malononitrile = 99% (Sigma-Aldrich), ethyl acetoacetate = 98% (Sigma-Aldrich), diethyl malonic acid = 97% (Sigma Aldrich), 4-fluroaniline and 3-trifluromethylaniline = 99% (Thermo Scientific UK), and 2-amino-1,1,3-propenetricarbonitrile = 97% (Sigma-Aldrich). According to solvents, ethanol is obtained as anhydrous pure ethanol = 99.99% (Fischer Scientific), and 1,4-dioxane = 97% (El-Nasr Pharmaceutical Chemicals). Using a solvent combination of DCM-MeOH (98-2) as the eluent, TLC was used to examine the synthesized compounds' purity on Merck precoated silica gel 60 F254 aluminum sheets. Spots were seen under 252 and 390 nm UV light. The cyanoacetamide derivatives, namely, 2-cyano-*N*-(4-fluorophenyl)acetamide (**A1**), 2-cyano-*N*-(3-(trifluoromethyl) phenyl)acetamide (**A2**), *N*-(4-chlorophenyl)-2-cyanoacetamide (**A3**), and ethyl 4-(2-cyanoacetamido)benzoate (**A4**) were prepared as the same method that described previously.[34,58,59]

4.1.2. Instrumental technique. All the recently developed compounds' melting points (MPs) were measured using open capillaries on a digital Gallen Kamp MFB-595. The IR Spectral were screened using KBr disk technique on a Shimadzu 440 spectrophotometer within the range of 400–4000 cm^{-1}. $^1H/^{13}C$ in the NMR spectra were obtained on a JOEL spectrometer 400/100 MHz, DMSO-d_6 were used as a solvent; chemical shifts were measured in δ ppm, relative to TMS as an internal standard ^1H NMR and ^{13}C NMR: 0.00 ppm. The Micro Analytical Unit at Cairo University in Cairo, Egypt, conducted the elemental analysis.

4.1.3. General reaction of starting material with different aliphatic activated methylene (2–5). A solution of 3-formyl-4-hydroxybenzenesulfonyl chloride (**1**) (2.19 g, 10.09 mmol), ammonium acetate (1.15 g, 15 mmol), and different acidic methylene (10.02 mmol), specified namely, malononitrile, 2-amino-1,1,3-propenetricarbonitrile, ethyl acetoacetate, and diethyl malonic acid in anhydrous pure ethanol (20 mL) and the reaction mixtures was stirred at 70 °C for 2–3.5 h until the dissolved clear solution is precipitated on hot. The different coloured solids were filtered off, purified with hot ethanol/dioxane, and air dried.

4.1.3.1. 3-Cyano-2-imino-2H-chromene-6-sulfonamide (2). Light-orange powder; m. p. = 190–192 °C, 91% yield; anal. calcd (%) for $C_{10}H_7N_3O_3S$ (249.24 g mol^{-1}): C, 48.19; H, 2.83; N, 16.86; found (%): C, 48.48; H, 2.70; N, 16.99; IR (KBr): ν_{max} = 3414, 3335, 3233 (NH & NH_2), 3080, (sp^2-CH), 2203 (CN), 1620 (C=NH), 1592 (C=C), 1399, 1185 (SO_2); ^1H NMR (δ, ppm) = 7.32 (d, *J* = 8.8 Hz, 1H, H_8-phenyl), 7.86 (dd, *J* = 8.4, 4.0 Hz, 1H, H_7-phenyl), 8.10 (s, 2H, NH_2), 8.39 (s, 1H, H_5-phenyl), 8.76 (s, 1H, H_4-pyran), 9.39 (s, 1H, NH); ^{13}C NMR (ppm) δ 96.01 (C–CN, C_3-pyran), 111.45 (C_4-pyran), 116.21 (CN), 118.25 (C-sp^2), 122.61(C-sp^2), 127.71(C-sp^2), 131.91(C-sp^2), 138.12 (C–SO_2), 157.90 (O–C=C), 160.53 (C=NH).

4.1.3.2. 3-(1-Amino-2,2-dicyanovinyl)-2-imino-2H-chromene-6-sulfonamide (3). Deep-orange powder; m. p. = 176–178 °C, 84% yield; anal. calcd (%) for $C_{13}H_9N_5O_3S$ (315.31 g mol^{-1}): C, 49.52; H, 2.88; N, 22.21; found (%): C, 49.23; H, 2.91; N, 22.11; IR (KBr): ν_{max} = 3418, 3336, 3227 (NH & $2NH_2$), 3040, (sp^2-CH), 2203 (CN), 1621 (C=NH), 1568 (C=C), 1400, 1185 (SO_2); ^1H NMR (δ, ppm) = 4.99 (s, 2H, NH_2), 6.94 (d, *J* = 8.0 Hz, 1H, H_8-phenyl), 7.40 (d, *J* = 8.4 Hz, 1H, H_7-phenyl), 7.53 (br.s, 2H, NH_2), 7.66 (s, 1H, H_5-phenyl), 7.95 (s, 1H, H_4-pyran), 8.07 (s, 1H, NH); ^{13}C NMR (ppm) δ 52.65 (C-$(CN)_2$), 113.48 (CN), 118.25 (C_4-pyran), 122.61 (C-sp^2), 127.71 (C-sp^2), 131.91 (C-sp^2), 136.68 (C-sp^2), 138.12 (C-sp^2), 140.05 (C–SO_2), 156.69 (O–C=C), 160.08 (C=NH), 178.95 (NH_2–C=C).

4.1.3.3. 3-Acetyl-2-oxo-2H-chromene-6-sulfonamide (4). Orange powder; m. p. = 151–153 °C, 78% yield; anal. calcd (%) for $C_{11}H_9NO_5S$ (267.26 g mol^{-1}): C, 49.44; H, 3.39; N, 5.24; found (%): C, 49.78; H, 3.15; N, 5.55; IR (KBr): ν_{max} = 3394, 3300 (NH_2), 3110 (sp^2-CH), 2980 (sp^3-CH), 1716 (2CO), 1563 (C=C), 1367, 1270 (SO_2); ^1H NMR (δ, ppm) = 2.31 (s, 3H, $COCH_3$), 6.70 (br.s, 2H, NH_2), 7.33 (d, *J* = 8.8 Hz, 1H, H_8-phenyl), 7.87 (d, *J* = 8.4 Hz, 1H, H_7-phenyl), 8.40 (s, 1H, H_5-phenyl), 8.74 (s, 1H, H_4-pyran); ^{13}C NMR (ppm) δ 25.90 (CO–CH_3), 119.54 (C-sp^2), 119.91

(C-sp^2), 122.06 (C-sp^2), 127.30 (C-sp^2), 131.65 (C-sp^2), 138.55 (C-sp^2), 144.90 (C–SO_2), 157.46 (O–C=C), 161.15 (C=O), 183.43 (CO–CH_3).

4.1.3.4. Ethyl 2-oxo-6-sulfamoyl-2H-chromene-3-carboxylate (5). Red powder; m. p. = 165–167 °C, 76% yield; anal. calcd (%) for $C_{12}H_{11}NO_6S$ (297.28 g mol^{-1}): C, 48.48; H, 3.73; N, 4.71; found (%): C, 48.43; H, 3.82; N, 4.75; IR (KBr): ν_{max} = 3183 (br.NH_2), 3064 (sp^2-CH), 1765, 1710 (2CO), 1570 (C=C), 1366, 1180 (SO_2); ^{1}H NMR (δ, ppm) = 1.29 (t, J = 6.0 Hz, 3H, CH_3CH_2O-), 4.27 (q, J = 5.6 Hz, 2H, CH_3CH_2O-), 6.78 (s, 2H, NH_2), 7.61 (d, J = 7.2 Hz, 1H, H_8-phenyl), 7.92 (d, J = 7.2 Hz, 1H, H_7-phenyl), 8.40 (s, 1H, H_5-phenyl), 8.96 (s, 1H, H_4-pyran); ^{13}C NMR (ppm) δ 13.99 (CH_3CH_2O-), 60.58 (CH_3CH_2O-), 118.26 (C-sp^2), 122.61 (C-sp^2), 125.61 (C-sp^2), 127.71 (C-sp^2), 131.91 (C-sp^2), 138.12 (C-sp^2), 140.33 (C–SO_2), 156.58 (O–C=C), 161.62 (C=O), 168.14 (CO–OEt).

4.1.4. General reaction of starting material with different cyanacetanilide (6–9). The appropriate ammonium acetate (1.15 g, 15 mmol), and different acidic methylene (10.02 mmol), namely, 2-cyano-*N*-(4-fluorophenyl)acetamide (**A1**), 2-cyano-*N*-(3-(trifluoromethyl) phenyl)acetamide (**A2**), *N*-(4-chlorophenyl)-2-cyanoacetamide (**A3**), and ethyl 4-(2-cyanoacetamido) benzoate (**A4**) were added to a solution of sulfonylchloride salicylaldehyde (**1**) (2.19 g, 10.09 mmol) in anhydrous pure ethanol (20 mL) at room temperature. The solution mixture was stirred at 70 °C for 3–5 hs until the dissolved clear solution is precipitated on hot (monitored by TLC). The different coloured solids were filtered off, purified with hot ethanol/acetic acid, and air dried.

4.1.4.1. N-(4-fluorophenyl)-2-oxo-6-sulfamoyl-2H-chromene-3-carboxamide (6). Light-red powder; m. p. = 215–217 °C, 67% yield; anal. calcd (%) for $C_{16}H_{11}FN_2O_5S$ (362.33 g mol^{-1}): C, 53.04; H, 3.06; N, 7.73; found (%): C, 53.24; H, 2.91; N, 7.66; IR (KBr): ν_{max} = 3431 (br.NH_2 & NH), 3097 (sp^2-CH), 1727 (CO), 1654 (CO–NH), 1605 (C=C), 1359, 1191 (SO_2); ^{1}H NMR (δ, ppm) = 6.90 (s, 2H, NH_2), 7.21 (d, J = 8.4 Hz, 2H, Ar–H), 7.69 (d, J = 9.2 Hz, 1H, H_8-phenyl), 7.72 (d, J = 8.8 Hz, 2H, Ar–H), 7.76 (d, J = 8.4 Hz, 1H, H_7-phenyl), 8.34 (s, 1H, H_5-phenyl), 8.43 (s, 1H, H_4-pyran), 10.46 (s, 1H, CO–NH); ^{13}C NMR (ppm) δ 115.30 (C-sp^2), 121.49 (C-sp^2), 124.45 (C-sp^2), 126.66 (C-sp^2), 127.33 (C-sp^2), 128.56 (C-sp^2), 129.43 (C-sp^2), 129.74 (C-sp^2), 130.60 (C-sp^2), 134.71 (C-sp^2), 146.68 (C-sp^2), 152.44 (C–SO_2), 156.92 (O–C=C), 161.85 (C–F), 162.61 (C=O), 166.15 (CO–NH); ^{19}F NMR (376 MHz, DMSO) δ −118.03 (s, 1F).

4.1.4.2. 2-Oxo-6-sulfamoyl-N-(3-(trifluoromethyl)phenyl)-2H-chromene-3-carboxamide (7). Deep-red powder; m. p. = 223–225 °C, 83% yield; anal. calcd (%) for $C_{17}H_{11}F_3N_2O_5S$ (412.34 g mol^{-1}): C, 49.52; H, 2.69; N, 7.79; found (%): C, 49.74; H, 2,79; N, 7.54; IR (KBr): ν_{max} = 3431 (br.NH_2 & NH), 3098 (sp^2-CH), 1727 (CO), 1654 (CO–NH), 1573 (C=C), 1360, 1191 (SO_2); ^{1}H NMR (δ, ppm) = 6.73 (s, 2H, NH_2), 7.23 (d, J = 6.8 Hz, 1H, Ar–H), 7.29–7.32 (m, 2H, Ar–H + H_8-phenyl), 7.48 (d, J = 6.8 Hz, 1H, Ar–H), 7.79 (d, J = 6.8 Hz, 1H, H_7-phenyl), 7.83–7.87 (m, 1H, Ar–H), 8.18 (s, 1H, H_5-phenyl), 8.36 (s, 1H, H_4-pyran), 9.37 (s, 1H, CO–NH); ^{13}C NMR (ppm) δ 111.70 (C-sp^2), 115.34 (C-sp^2), 115.62 (C-sp^2), 118.63 (C-sp^2), 119.07 (C-sp^2), 121.37 (C-sp^2), 123.20 (C-sp^2), 124.25 (C–F_3), 125.82 (C-sp^2), 127.49 (C-sp^2), 129.64 (C-sp^2), 133.33 (C-sp^2), 136.44 (C-sp^2), 144.24 (C–SO_2), 155.30 (O–C=C), 159.38 (C=O), 164.34 (CO–NH); ^{19}F NMR (376 MHz, DMSO) δ/ppm −61.29 (s, 3F).

4.1.4.3. N-(4-chlorophenyl)-2-oxo-6-sulfamoyl-2H-chromene-3-carboxamide (8). Deep-yellow powder; m. p. = 209–211 °C, 77% yield; anal. calcd (%) for $C_{16}H_{11}ClN_2O_5S$ (378.78 g mol^{-1}): C, 50.74; H, 2.93; N, 7.40; found (%): C, 50.82; H, 2.86; N, 7.45; IR (KBr): ν_{max} = 3430 (br.NH_2 & NH), 3104 (sp^2-CH), 1726 (CO), 1654 (CO–NH), 1573 (C=C), 1380, 1137 (SO_2); ^{1}H NMR (δ, ppm) = 6.72 (s, 2H, NH_2), 7.32 (d, J = 8.8 Hz, 2H, Ar–H), 7.51 (d, J = 8.4 Hz, 1H, H_8-phenyl), 7.81 (d, J = 10.4 Hz, 1H, Ar–H), 7.86 (d, J = 6.4 Hz, 1H, Ar–H), 7.98 (d, J = 8.8 Hz, 1H, H_7-phenyl), 8.10 (s, 1H, H_5-phenyl), 8.39 (s, 1H, H_4-pyran), 9.38 (s, 1H, CO–NH); ^{13}C NMR (ppm) δ 114.19 (C-sp^2), 116.83 (C-sp^2), 117.77 (C-sp^2), 118.61 (C-sp^2), 119.57 (C-sp^2), 122.40 (C-sp^2), 126.33 (C-sp^2), 128.50 (C-sp^2), 130.57 (C-sp^2), 131.16 (C-sp^2), 133.84 (C-sp^2), 134.88 (C-sp^2), 142.41 (C–SO_2), 153.98 (O–C=C), 159.44 (C=O), 164.09 (CO–NH).

4.1.4.4. Ethyl 4-(2-oxo-6-sulfamoyl-2H-chromene-3-carboxamido)benzoate (9). Pale-orange powder; m. p. = 233–235 °C, 86% yield; anal. calcd (%) for $C_{19}H_{16}N_2O_7S$ (416.40 g mol^{-1}): C, 54.80; H, 3.87; N, 6.73; found (%): C, 54.82; H, 3.88; N, 6.68; IR (KBr): ν_{max} = 3430 (br.NH_2 & NH), 3073 (sp^2-CH), 1726 (2CO), 1655 (CO–NH), 1572 (C=C), 1361, 1192 (SO_2); ^{1}H NMR (δ, ppm) = 1.24 (t, J = 7.2 Hz, 3H, CH_3CH_2O-), 4.18 (q, J = 5.6 Hz, 2H, CH_3CH_2O-), 5.91 (s, 2H, NH_2), 6.53 (d, J = 8.4 Hz, 2H, Ar–H), 6.92 (d, J = 6.4 Hz, 1H, H_8-phenyl), 7.51 (d, J = 6.8 Hz, 1H, H_7-phenyl), 7.60 (d, J = 6.8 Hz, 2H, Ar–H), 7.86 (s, 1H, H_5-phenyl), 7.99 (s, 1H, H_4-pyran), 10.23 (s, 1H, CO–NH); ^{13}C NMR (ppm) δ 14.76 (CH_3CH_2O-), 61.03 (CH_3CH_2O-), 115.07 (C-sp^2), 115.52 (C-sp^2), 116.76 (C-sp^2), 120.77 (C-sp^2), 124.50 (C-sp^2), 127.35 (C-sp^2), 128.87 (C-sp^2), 130.59 (C-sp^2), 132.14 (C-sp^2), 134.05 (C-sp^2), 138.30 (C-sp^2), 140.18 (C-sp^2), 144.61 (C–SO_2), 155.12 (O–C=C), 157.58 (C=O), 163.46 (CO–NH), 166.20 (CO–OEt).

4.2. Biological evaluation

4.2.1. *In vitro* α-amylase inhibitory assay. The *in vitro* α-amylase inhibitory activity for the designed 6-sulfonyl chromene derivatives **2–9** was carried out using BioVision's α-Amylase Inhibitor Screening Kit (Catalog #K482-100) and with the help of multi-well spectrophotometer (ELISA reader) using 96 well microplate at (OD = 405 nm) according to manufacturer's instructors as described previously[60] (all details and raw material data presented in ESI file†).

4.2.2. *In vitro* α-glucosidase inhibitory assay. The α-glucosidase inhibitory activity of most active 6-sulfonyl chromene derivatives **2** and **9** was performed using BioVision's α-Glucosidase Inhibitor Screening Kit (Colorimetric) (Catalog #K938-100) at (OD: 410 nm) and the results read on multi-well spectrophotometer (ELISA reader) using 96 well microplate according to manufacturer's instructors as described previously[61] (all details and raw material data presented in ESI file†).

4.2.3. *In vitro* PPAR-γ inhibitory assay. By using Human PPAR-γ (Peroxisome Proliferator-Activated Receptor Gamma) ELISA Kit Catalog No: MBS2503174 and according to the manufacturer's instructors, the *in vitro* PPAR-γ activity of most

active 6-sulfonyl chromene derivatives **2** and **9** were evaluated by determining the IC_{50} (mg mL^{-1}) in comparison to Pioglitazone as a positive control as described previously.[62]

4.3. Molecular docking simulation

To determine the binding mode pattern for the most active chromene derivatives 2 and 9, the docking simulation conducted inside the active site of α-amylase (PDB: 2QV4, chain A), α-glucosidase (PDB: 3w37, chain A), and PPAR-γ (PDB: 3SZ1, chain B) as described previously.[55–57] The 3D structure of proteins was obtained from the protein data bank (**https://www.rcsb.org/**), and each protein was prepared by default protocol where the water molecules were removed, and only one chain was selected for docking purposes. The active site was protonated, then the energy was minimized using MMFF94X with a gradient of 0.05 kcal mol^{-1} and saved as an mdb file.[63,64] The structure of most active 6-sulfamoyl-2*H*-chromene derivatives **2** and **9**, as well as Pioglitazone were drawn and constructed using chembiodraw14, then prepared by protonation and minimized using standard protocol for MOE as described previously.[65–67]

Conflicts of interest

The authors declare no conflicts of interest.

Acknowledgements

The authors extend their appreciation to the Deanship of Scientific Research at Northern Border University for funding this work through research group no. (RG-NBU-2022-1705).

References

1 N. H. Cho, J. E. Shaw, S. Karuranga, Y. Huang, J. D. da Rocha Fernandes, A. W. Ohlrogge and B. Malanda, *Diabetes Res. Clin. Pract.*, 2018, **138**, 271–281.
2 A. D. Association, *Diabetes Care*, 2013, **37**, S81–S90.
3 Z. D. Kifle, M. Abdelwuhab, A. D. Melak, G. Genet, T. Meseret and M. Adugna, *Metab. Open*, 2022, **13**, 100174.
4 P. O. U. Adogu, H. N. Chineke, M. U. Ewuzie, O. O. Enwere and N. B. Egenti, *J. Diabetes Mellitus*, 2015, **5**, 49.
5 A. Ali, F. Iqbal, A. Taj, Z. Iqbal, M. J. Amin and Q. Z. Iqbal, *Pak. J. Med. Sci.*, 2013, **29**, 899–902.
6 D. Care, *Diabetes Care*, 2017, **40**, S11–S24.
7 A. E. Kitabchi, G. E. Umpierrez, M. B. Murphy and R. A. Kreisberg, *Diabetes Care*, 2006, **29**, 2739–2748.
8 S. S. S. Surya, A. D. Salam, D. V Tomy, B. Carla, R. A. Kumar and C. S. C. Sunil, *Int. J. Pharm. Biomed. Sci.*, 2014, **4**, 337–347.
9 D. K. Patel, R. Kumar, D. Laloo and S. Hemalatha, *Asian Pac. J. Trop. Biomed.*, 2012, **2**, 411–420.
10 M. Przeor, *Pharmaceuticals*, 2022, **15**, 65.
11 P. Subash Babu, S. Prabuseenivasan and S. Ignacimuthu, *Phytomedicine*, 2007, **14**, 15–22.
12 L. Pari and N. Rajarajeswari, *Chem.-Biol. Interact.*, 2009, **181**, 292–296.
13 S. M. Patil, R. M. Martiz, A. M. Satish, A. M. Shbeer, M. Ageel, M. Al-Ghorbani, L. Ranganatha, S. Parameswaran and R. Ramu, *Molecules*, 2022, **27**, 3888.
14 S. M. Patil, R. M. Martiz, R. Ramu, P. S. Shirahatti, A. Prakash, B. R. P. Kumar and N. Kumar, *J. Biomol. Struct. Dyn.*, 2022, **40**, 12491–12505.
15 A. J. Scheen, *Diabet. Epidemiol. Manag.*, 2023, **11**, 100145.
16 M. S. Asgari, M. Mohammadi-Khanaposhtani, M. Kiani, P. R. Ranjbar, E. Zabihi, R. Pourbagher, R. Rahimi, M. A. Faramarzi, M. Biglar, B. Larijani, M. Mahdavi, H. Hamedifar and M. H. Hajimiri, *Bioorg. Chem.*, 2019, **92**, 103206.
17 D. Egan, R. O'kennedy, E. Moran, D. Cox, E. Prosser and R. D. Thornes, *Drug Metab. Rev.*, 1990, **22**, 503–529.
18 J. V Patil, S. S. Soman, S. Umar, P. Girase and S. Balakrishnan, *ChemistrySelect*, 2024, **9**, e202303391.
19 E. A. Fayed, M. Mohsen, S. M. A. El-Gilil, D. S. Aboul-Magd and A. Ragab, *J. Mol. Struct.*, 2022, **1262**, 133028.
20 N. Q. Khai and T. K. Vu, *Anti-Cancer Agents Med. Chem.*, 2024, **24**, 18–29.
21 A. Ibrar, S. A. Shehzadi, F. Saeed and I. Khan, *Bioorg. Med. Chem.*, 2018, **26**, 3731–3762.
22 Q. Shen, J. Shao, Q. Peng, W. Zhang, L. Ma, A. S. C. Chan and L. Gu, *J. Med. Chem.*, 2010, **53**, 8252–8259.
23 V. Channabasappa, K. Kumara and A. K. Kariyappa, *J. Chem. Sci.*, 2021, **133**, 130.
24 S. Gorain, J. Pal and S. J. Biswas, in *Antidiabetic Medicinal Plants*, ed. M. Naeem and T. Aftab, Academic Press, 2024, pp. 141–166.
25 S. Shahdadi, F. Hamidi and B. Fathi, *Heliyon*, 2024, **10**, e24436.
26 V. Kumar, D. Ahmed, A. Verma, F. Anwar, M. Ali and M. Mujeeb, *BMC Complementary Altern. Med.*, 2013, **13**, 273.
27 H. Sun, X. Song, Y. Tao, M. Li, K. Yang, H. Zheng, Z. Jin, R. H. Dodd, G. Pan, K. Lu and P. Yu, *Future Med. Chem.*, 2018, **10**, 1055–1066.
28 M. S. Asgari, M. Mohammadi-Khanaposhtani, M. Kiani, P. Rashidi Ranjbar, E. Zabihi, R. Pourbagher, R. Rahimi, M. A. Faramarzi, M. Biglar, B. Larijani, M. Mahdavi, H. Hamedifar and M. H. Hajimiri, *Bioorg. Chem.*, 2018, **92**, 103206.
29 E. Elahabaadi, A. A. Salarian and E. Nassireslami, *Polycyclic Aromat. Compd.*, 2022, **42**, 4317–4327.
30 E. L. R. Stokstad and T. H. Jukes, *J. Nutr.*, 1987, **117**, 1335–1341.
31 M. N. L. Nalam, A. Peeters, T. H. M. Jonckers, I. Dierynck and C. A. Schiffer, *J. Virol.*, 2007, **81**, 9512–9518.
32 Y. L. Hong, P. A. Hossler, D. H. Calhoun and S. R. Meshnick, *Antimicrob. Agents Chemother.*, 1995, **39**, 1756–1763.
33 A. Ragab, S. A. Fouad, O. A. A. Ali, E. M. Ahmed, A. M. Ali, A. A. Askar and Y. A. Ammar, *Antibiotics*, 2021, **10**, 162.
34 R. R. Raslan, Y. A. Ammar, S. A. Fouad, S. A. Hessein, N. A. M. Shmiess and A. Ragab, *RSC Adv.*, 2023, **13**, 10440–10458.

35 M. A. Ismail, M. S. Abusaif, M. S. A. El-Gaby, Y. A. Ammar and A. Ragab, *RSC Adv.*, 2023, **13**, 12589–12608.
36 F. Carta, C. T. Supuran and A. Scozzafava, *Future Med. Chem.*, 2014, **6**, 1149–1165.
37 M. A. Gouda and B. H. M. Hussein, *Lett. Drug Des. Discovery*, 2017, **14**, 1425–1432.
38 A. Markham, *Drugs*, 2017, **77**, 697–704.
39 H. A. Mohamed, Y. A. Ammar, G. A. M. Elhagali, H. A. Eyada, D. S. Aboul-Magd and A. Ragab, *J. Mol. Struct.*, 2023, **1287**, 135671.
40 M. S. A. El-Gaby, Y. A. Ammar, M. A. Ismail, A. Ragab and M. S. Abusaif, *Heterocycl. Commun.*, 2023, **29**, 20220170.
41 Y. A. Ammar, A. Ragab, M. A. Migahed, S. Al-Sharbasy, M. A. Salem, O. K. M. Riad, H. M. R. M. Selim, G. A. Abdelmaksoud and M. S. Abusaif, *RSC Adv.*, 2023, **13**, 27363–27384.
42 K. Zessel, S. Mohring, G. Hamscher, M. Kietzmann and J. Stahl, *Chemosphere*, 2014, **100**, 167–174.
43 V. Garaj, L. Puccetti, G. Fasolis, J.-Y. Winum, J.-L. Montero, A. Scozzafava, D. Vullo, A. Innocenti and C. T. Supuran, *Bioorg. Med. Chem. Lett.*, 2005, **15**, 3102–3108.
44 U. Košak, B. Brus, D. Knez, R. Šink, S. Žakelj, J. Trontelj, A. Pišlar, J. Šlenc, M. Gobec, M. Živin, L. Tratnjek, M. Perše, K. Sałat, A. Podkowa, B. Filipek, F. Nachon, X. Brazzolotto, A. Więckowska, B. Malawska, J. Stojan, I. M. Raščan, J. Kos, N. Coquelle, J.-P. Colletier and S. Gobec, *Sci. Rep.*, 2016, **6**, 39495.
45 M. Bavadi, K. Niknam and O. Shahraki, *J. Mol. Struct.*, 2017, **1146**, 242–253.
46 R. Schobert, R. Stehle and H. Walter, *Tetrahedron*, 2008, **64**, 9401–9407.
47 D. Borah, P. N. Bhattacharyya, B. C. Nath, R. Chetia, N. F. Islam, B. Sarma and J. Fluor, *Chem*, 2024, **274**, 110259.
48 M. Kou, J. Zheng, T. Chen, Y. Wu, L. Huang, D. Cao, D. Chen and J. Fluor, *Chem*, 2024, **276**, 110279.
49 Y. A. Ammar, J. A. Micky, D. S. Aboul-Magd, S. M. A. Abd El-Hafez, S. A. Hessein, A. M. Ali and A. Ragab, *Chem. Biol. Drug Des.*, 2023, **101**, 245–270.
50 M. M. Abdelgalil, Y. A. Ammar, G. A. M. Elhag Ali, A. K. Ali and A. Ragab, *J. Mol. Struct.*, 2023, **1274**, 134443.
51 A. Ragab, M. S. Abusaif, N. A. Gohar, D. S. Aboul-Magd, E. A. Fayed and Y. A. Ammar, *Bioorg. Chem.*, 2023, **131**, 106307.
52 A. Ragab, S. A. Ibrahim, D. S. Aboul-Magd and M. H. Baren, *RSC Adv.*, 2023, **13**, 34756–34771.
53 A. Ragab, M. S. Abusaif, D. S. Aboul-Magd, M. M. S. Wassel, G. A. M. Elhagali and Y. A. Ammar, *Drug Dev. Res.*, 2022, 1305–1330.
54 R. Ayman, M. S. Abusaif, A. M. Radwan, A. M. Elmetwally and A. Ragab, *Eur. J. Med. Chem.*, 2023, **249**, 115138.
55 Y. M. Abdel-Baky, A. M. Omer, E. M. El-Fakharany, Y. A. Ammar, M. S. Abusaif and A. Ragab, *Sci. Rep.*, 2023, **13**, 22792.
56 A. S. Hassan, N. M. Morsy, W. M. Aboulthana and A. Ragab, *Drug Dev. Res.*, 2023, **84**, 3–24.
57 V. M. Patil, K. N. Tilekar, N. M. Upadhyay and C. S. Ramaa, *ChemistrySelect*, 2022, **7**, e202103848.
58 K. E. Saadon, N. M. H. Taha, N. A. Mahmoud, G. A. M. Elhagali and A. Ragab, *J. Iran. Chem. Soc.*, 2022, **19**, 3899–3917.
59 A. Ragab, S. A. Fouad, Y. A. Ammar, D. S. Aboul-Magd and M. S. Abusaif, *Antibiotics*, 2023, **12**, 128.
60 M. J. Mphahlele, N. M. Magwaza, S. T. Malindisa and Y. S. Choong, *Chem. Biol. Drug Des.*, 2021, **98**, 234–247.
61 S. H. Aly, A. M. Elissawy, M. A. El Hassab, T. A. Majrashi, F. E. Hassan, E. B. Elkaeed, W. M. Eldehna and A. N. B. Singab, *J. Enzyme Inhib. Med. Chem.*, 2024, **39**, 2292482.
62 E. A. Fayed, A. Thabet, S. M. A. El-Gilil, H. M. A. Elsanhory and Y. A. Ammar, *J. Mol. Struct.*, 2024, **1301**, 137374.
63 R. Ayman, A. M. Radwan, A. M. Elmetwally, Y. A. Ammar and A. Ragab, *Arch. Pharm.*, 2023, **356**, e2200395.
64 M. Basseem, A. A. Emam, F. H. Kamal, A. M. Gamal and S. A. Abo Faraha, *Appl. Organomet. Chem.*, 2023, **37**, 1–23.
65 H. F. Rizk, M. A. El-Borai, A. Ragab, S. A. Ibrahim and M. E. Sadek, *Polycyclic Aromat. Compd.*, 2023, **43**, 500–522.
66 S. A. Ibrahim, A. Ragab and H. A. El-Ghamry, *Appl. Organomet. Chem.*, 2022, **36**, e6508.
67 E. S. A. E. H. Khattab, A. Ragab, M. A. Abol-Ftouh and A. A. Elhenawy, *J. Biomol. Struct. Dyn.*, 2022, **40**, 13291–13309.